6

Rotating Ring-Disk Electrodes

Fundamentals of the Digital Simulation Approach. Disk and Ring Transients and Collection Efficiencies

Keith B. Prater[1] and Allen J. Bard*

Department of Chemistry, The University of Texas at Austin, Austin

ABSTRACT

A digital simulation technique has been used to treat electrode reactions occurring at the rotating ring-disk electrode (RRDE). The method of treating normal diffusion, normal and radial convection, and homogeneous kinetics at the RRDE is discussed and results for the transient and steady-state currents at the disk and ring electrodes in the absence of kinetic complications are given. Where comparisons are possible, the simulated results were found to be in excellent agreement with previous theoretical treatments.

The rotating ring-disk electrode (RRDE) was introduced in 1959 by Frumkin and Nekrasov (1). The addition of a ring electrode to the rotating disk electrode permitted the detection of products formed by electrode reactions and provided a steady-state method for investigating coupled chemical reactions. However, the mass transfer conditions existing at the RRDE are rather complex, and the mathematical treatment of the RRDE, especially in the presence of kinetic complications, is difficult. A general mathematical treatment was not given until 1966 when a series of papers by Albery and Bruckenstein (2-9) appeared. In these papers, Albery and Bruckenstein presented an exact treatment of the steady-state collection efficiency as a function of electrode geometry in the absence of kinetic complications (3). They also presented approximate treatments of first- and second-order follow up reactions. Unfortunately, as pointed out by Albery (10), the treatment of the first-order case is not applicable to any practical electrode without further approximations. Their second-order treatment is limited to certain regions of rotation rate and rate constant. Furthermore, expansion of these treatments to more complex mechanisms, such as ECE reactions and electrogenerated chemiluminescence (11), seems unlikely.

In this series of papers, we present the results of the application of a digital simulation technique to this problem. This technique is capable of generating a theoretical working curve for any particular electrode under any imaginable kinetic situation. The simulation technique used is a modification of that introduced to electrochemical problems by Feldberg (12) and most fully described in a recent chapter (13). This paper also discusses the mathematical background of the method and gives a detailed description of other applications of this technique.

The principal problem encountered in simulating the RRDE is that, due to the normal and radial convective flow, the concentrations of all species are functions of two spatial variables, X, the normal distance from the electrode surface, and R, the radial distance from the axis of rotation. It is here that this paper differs from those previously presented.

Digital Simulation Method

Digital model.—In a digital simulation of an electrochemical system, one first divides the solution into a number of small volume elements. These volume elements will henceforth be called "boxes" regardless of shape. The shapes of these boxes are chosen in such a way that one can reasonably assume that the solution within each box is homogeneous. For an RRDE, the symmetry of the system suggests the following model. The solution is first divided into thin parallel layers which are Δx cm thick. The electrode is placed in the center of the first layer, parallel to the planes dividing the layers. Then each layer is divided into a cylindrical box of radius $\frac{1}{2}\ \Delta r$ cm which is centered about the axis of rotation, and a series of concentric annular boxes Δr cm wide (Fig. 1). The parameter, Δr, is chosen in such a way that the pertinent radii of

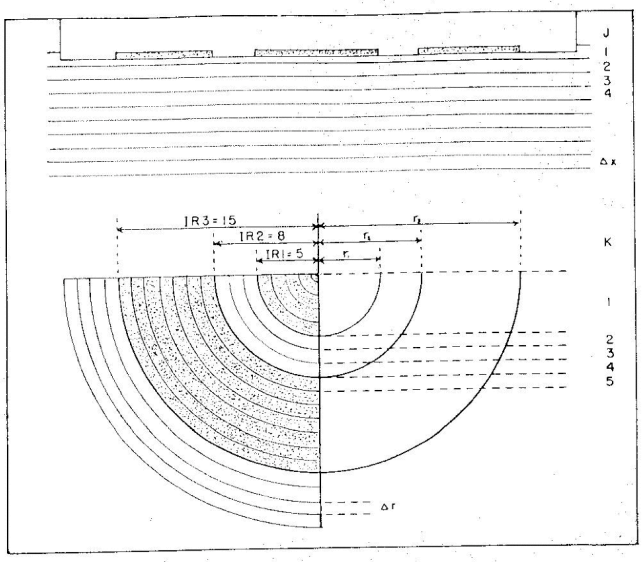

Fig. 1. Digital simulation model of the rotating ring disk electrode.

the electrode, r_1 (the radius of the disk electrode), r_2 (the radius to the inner edge of the ring electrode), and r_3 (the radius to the outer edge of the ring electrode), can be satisfactorily approximated by

$$r_1 = (IR1\text{-}0.5)(\Delta r)$$
$$r_2 = (IR2\text{-}0.5)(\Delta r)$$
$$r_3 = (IR3\text{-}0.5)(\Delta r) \qquad [1]$$

where $IR1$, $IR2$, and $IR3$ are integers and correspond to the number of boxes necessary to represent the particular radial distances. Obviously, the smaller Δr is (*i.e.*, the greater the number of annular boxes), the better the approximation is likely to be. Unfortunately, the number of boxes must be weighed against the length of computation time and some compromise reached.

In the interest of minimizing computation time, one can very reasonably assume that the disk electrode is a uniformly accessible surface. This condition holds under usual experimental conditions where an excess of supporting electrolyte is present (14). This means that in each layer, the solution in the cylindrical volume of radius $(IR1\text{-}0.5)(\Delta r)$ centered about the axis of rotation is homogeneous and can be represented by one large cylindrical box.

For the sake of simplicity the following convention is used. Each box is referred to by its layer number, J, and its radial number, K. The layer containing the electrode is the $J = 1$ layer, and all other layers are numbered consecutively outward from the electrode. Within any layer, the large central cylindrical box is called the $K = 1$ box, and all the annular boxes are numbered consecutively outward from this box. The large cylindrical box in the first layer ($J = 1$, $K = 1$) corresponds to the disk electrode. Similarly, the appropriate first layer ($J = 1$) annular boxes correspond to the gap region, the ring electrode region, or the outer insulation region.

A concentration for each of the active species in solution is then assigned to each box. This concentration is associated with the center of each box. Thus, in the particular case of the boxes in the first layer, the concentrations in those boxes correspond to the concentrations at the electrode surface. Before electrolysis begins, all boxes are assigned concentrations which correspond to the bulk concentration of the solution. At the beginning of electrolysis, $t = 0$, the concentrations in those first layer boxes corresponding to the disk and ring electrodes are changed to reflect appropriate boundary conditions. These changes result in a concentration gradient between some of the corresponding boxes in the first and second layers. Using a finite difference representation of Fick's second law, the extent to which the concentrations in these boxes are changed by diffusion across the boundary between them in a time interval, Δt, is calculated. These changes in the original array of concentrations produce a new array reflecting the effects of diffusion during this first time interval. In all calculations we assume, following the arguments of Albery and Bruckenstein (3), that radial diffusion is negligible when compared with radial convection.

In the case of a rotating electrode, convection is also taking place during the same time interval, Δt. From the treatment by Levich (15) of convection to a rotating disk electrode one can calculate the normal and radial components of fluid velocity at any point near the electrode. Thus, one can calculate the distance a given fluid volume will travel in the normal and radial directions in a time, Δt. If, for example, this calculation reveals that the volume element in the Kth ring of the Jth layer at the end of Δt seconds has traveled a distance ΔJ in the normal direction and a distance ΔK in the radial direction, then by replacing the concentration in the J, Kth box in the existing array with the concentration at $J + \Delta J$, $K - \Delta K$, a new array is generated which reflects the effects of both diffusion and convection for a time Δt.

If, in addition, one or more species undergo homogeneous reactions, this can be simulated by calculating, for each box containing the appropriate species, the amount by which each species will be depleted or increased according to the appropriate rate law in a time Δt. This generates an array which represents the expected concentration profile of the simulated system at a time Δt after the initiation of electrolysis. From this profile, the current observed at this point in an experiment can be calculated by assuming that the current is proportional to the difference between the concentrations in the corresponding boxes in the first and second layers, *i.e.*, the flux at the electrode surface. After making the adjustments to the concentrations in the appropriate boxes due to the passage of current, the above process is repeated to give a new concentration profile and current at $t = 2\Delta t$ and so on until the steady state has been attained. In the limit, as $\Delta x \to 0$, $\Delta t \to 0$, and $\Delta r \to 0$, the calculated current-time behavior and the steady-state currents should approach those observed experimentally.

Initial and boundary conditions.—Let us now consider the simulation in greater detail by discussing the following situation. The solution initially contains only species A at bulk concentration C°_A. At time $t = 0$, the potential of the disk electrode is stepped to a potential on the limiting current plateau for the reaction

$$A \pm ne \to B \qquad [2]$$

We consider the case where species B undergoes a first order homogeneous reaction to give some electroinactive species, X, by the reaction

$$B \xrightarrow{k_1} X \qquad [3]$$

The potential of the ring electrode is such that all B reaching the ring electrode is instantaneously converted back to A by

$$B \mp ne \to A \qquad [4]$$

In digital simulations, to make each computation as general as possible, all calculations are done in terms of dimensionless parameters. Hence, all concentrations are normalized with respect to the initial concentration of bulk species A. Thus, the initial fractional concentration of species A in any box is

$$F_A(J,K) = C^\circ_A/C^\circ_A = 1.0 \qquad [5]$$

and the fractional concentrations of species B and X are

$$F_B(J,K) = 0.0$$
$$F_X(J,K) = 0.0 \quad [6]$$

At the initiation of electrolysis, $t = 0$, the boundary conditions for the disk box in the case of a potential step to the limiting current region are

$$F_A(1,1) = 0.0$$
$$F_B(1,1) = 1.0$$
$$F_X(1,1) = 0.0 \quad [7]$$

For those first layer boxes which correspond to the ring electrode, the initial boundary conditions are

$$F_A(1,K_R) = 1.0$$
$$F_B(1,K_R) = 0.0$$
$$F_X(1,K_R) = 0.0 \quad [8]$$

where K_R represents all values of K corresponding to the ring electrode region.

Diffusion effects.—These conditions set up a concentration gradient between the first and second layer disk boxes ($J = 1$, $K = 1$) and ($J = 2$, $K = 1$), which gives rise to diffusion across the boundary between these boxes. The amount of material crossing the boundary in Δt seconds can be calculated using the finite difference representation of Fick's second law

$$\Delta F_A(J,K) = DM_A[F_A(J+1) - F_A(J,K)] - DM_A[F_A(J,K) - F_A(J-1,K)] \quad [9]$$

or

$$\Delta F_A(J,K) = DM_A[F_A(J+1,K) - 2F_A(J,K) + F_A(J-1,K)] \quad [10]$$

This states that for any time interval, Δt, the change in the fractional concentration of species A in the J,Kth box is the difference between the amount of A entering from the adjacent box of higher concentration and the amount of A going into the adjacent box of lower concentration. The amount entering or leaving the box is proportional to the concentration gradient across the boundary. The proportionality factor, DM_A is given by

$$DM_A = D_A \Delta t/(\Delta X)^2 \quad [11]$$

where D_A is the diffusion coefficient of species A and ΔX is the width of one layer. The parameter, Δt, is defined below. By applying Eq. [10] to all boxes and then replacing $F_A(J,K)$ by $F_A(J,K) + \Delta F_A(J,K)$, a new array of concentrations is generated which represents the effects of diffusion for a time interval Δt. The concentrations of species B and X are similarly treated. For this technique to converge, DM_A must have a value less than 0.5 (13). In most of these calculations, DM_A was taken to be 0.45.

Convection effects.—The parameter, Δt, is the real time length of one iteration. Thus

$$\Delta t = t_k/L \quad [12]$$

where t_k is some experimentally known time or time dimensioned variable, and L is the number of iterations used to simulate that time. To evaluate the appropriate form of t_k, consider the equation for the velocity of convective fluid flow in the direction normal to the electrode. In the region near the electrode, this is given by (15)

$$v_X = -0.51\,\omega^{3/2}\,\nu^{-1/2}\,X^2 \quad [13]$$

where ω is the rotation rate in radians/second, ν is the kinematic viscosity in square centimeters per second, and X is the distance from the electrode surface. The velocity in the X direction may be represented by the derivative, dX/dt. Thus

$$dX/dt = -0.51\,\omega^{3/2}\,\nu^{-1/2}\,X^2 \quad [14]$$

Solving the above, for X and evaluating between t_2 and t_1, one obtains

$$\frac{1}{X_2} - \frac{1}{X_1} = -0.51\,\omega^{3/2}\,\nu^{-1/2}\,(t_2 - t_1) \quad [15]$$

If we let $t_2 - t_1 = \Delta t$, then X_1 and X_2 represent the distance of a particular solution volume from the electrode surface at the beginning and end of the time interval, Δt. In terms of the layer number, J, the distance from the electrode surface to the center of any box is given by $(J - 1)(\Delta X)$. Let

$$XJ = J - 1 \quad [16]$$

and

$$X_1 = XJ(\Delta X) \quad [17]$$

then X_2 is the position in the old array of the solution volume which will be in the center of the Jth box at the end of the time interval, Δt. It is convenient to let

$$X_2 = (XJJ)\Delta X \quad [18]$$

where XJJ is a nonintegral distance from the electrode expressed in terms of numbers of boxes.

We can now rewrite Eq. [15] as

$$\frac{1}{XJJ} - \frac{1}{XJ} = -0.51\,\omega^{3/2}\,\nu^{-1/2}\,\Delta X\,\Delta t \quad [19]$$

or

$$XJJ = XJ/[1 - (XJ)(0.51\,\omega^{3/2}\,\nu^{-1/2}\,\Delta X \Delta t)] \quad [20]$$

The product $(0.51\,\omega^{3/2}\,\nu^{-1/2}\,\Delta X \Delta t)$ is dimensionless and is designated V_{NAUT}, that is

$$V_{NAUT} = 0.51\,\omega^{3/2}\,\nu^{-1/2}\,\Delta X \Delta t \quad [21]$$

From Eq. [11]

$$\Delta X = (D_A \Delta t/DM_A)^{1/2} \quad [22]$$

Thus

$$V_{NAUT} = 0.51\,\omega^{3/2}\,D_A^{1/2}\,\nu^{-1/2} DM_A^{-1/2} \Delta t^{3/2}$$

Using Eq. [12]

$$V_{NAUT} = 0.51\,\omega^{3/2}\,D_A^{1/2}\,\nu^{-1/2}\,DM_A^{-1/2}\,t_k^{3/2}\,L^{-3/2} \quad [24]$$

Letting

$$t_k = \omega^{-1}\,\nu^{1/3}\,D_A^{-1/3}\,(0.51)^{-2/3}$$

$$V_{NAUT} = DM_A^{-1/2}\,L^{-3/2} \quad [26]$$

then

$$XJJ = XJ/[1 - (XJ)(V_{NAUT})] \quad [27]$$

Note that the above substitutions render the calculation of the effects of convection not only dimensionless, but also strictly in terms of simulation variables. By replacing the concentrations now at the center of each box with the concentrations at the distance calculated from Eq. [27], a new array representing the effects of diffusion and convection normal to the electrode for a time, Δt, is generated.

In a similar manner, the effects of convection in the radial direction can be calculated. Beginning with the equation for fluid velocity in the radial direction near the electrode (15)

$$v_R = -0.51\,\omega^{3/2}\,\nu^{-1/2}\,XR \quad [28]$$

where R is the distance from the axis of rotation, one obtains

$$dR/dt = -0.51\,\omega^{3/2}\,\nu^{-1/3}\,XR \quad [29]$$

Solving Eq. [29] one obtains

$$\ln(R_2) - \ln(R_1) = -0.51\,\omega^{3/2}\,\nu^{-1/2}\,X\,(t_2 - t_1) \quad [30]$$

As before, R_2 and R_1 are the positions of a solution volume at times t_2 and t_1. Rearranging and substituting for X and $(t_2 - t_1)$

$$\ln(R_1/R_2) = 0.51\,\omega^{3/2}\,\nu^{-1/2}\,XJ\,\Delta X\,\Delta t \quad [31]$$

If we let

$$R_1 = RK(\Delta r) \quad [32]$$

and

$$R_2 = RKK(\Delta r) \quad [33]$$

and combine terms, we get

$$\ln(RK/RKK) = (V_{NAUT})(XJ)$$

and finally

$$RKK = RK \exp\left[-(V_{NAUT})(XJ)\right] \quad [35]$$

where

$$RK = K + IR1 - 2 \quad [36]$$

and is the radial distance of the solution volume in the center of the Kth box from the axis of rotation. RKK is the present position of the solution volume which will be at RK at the end of the Δt interval. Equation [35] allows the generation of an array of concentrations which represents the effects of diffusion and both normal and radial convection for a time, Δt.

Kinetic effects.—For a first order disappearance of species B from the J, Kth box, one can write the rate law in the form

$$\Delta C_B(J,K)/\Delta t = -kC_B(J,K) \quad [37]$$

Normalizing the concentrations by dividing both sides of the equation by C^o_A, and remembering that $F_B(J,K) = C_B(J,K)/C^o_A$, we have

$$\Delta F_B(J,K) = -k\Delta t\, F_B(J,K) \quad [38]$$

or substituting for Δt

$$\Delta F_B(J,K) = -[k\omega^{-1}\nu^{-1/3} D_A^{-1/3}(0.51)^{-2/3}]F_B(J,K)/L \quad [39]$$

The dimensionless collection of terms in brackets in Eq. [39] is called XKT, so that

$$XKT = k\omega^{-1}\nu^{1/3} D_A^{-1/3}(0.51)^{-2/3} \quad [40]$$

This is the dimensionless rate parameter which is used in the calculations. Rewriting Eq. [39], we get

$$\Delta F_B(J,K) = -XKT[F_B(J,K)]/L \quad [41]$$

Similarly, the expression for the appearance of species X is

$$\Delta F_X(J,K) = XKT[F_B(J,K)]/L = -\Delta F_B(J,K) \quad [42]$$

By replacing $F_B(J,K)$ with $F_B(J,K) + \Delta F_B(J,K)$ and $F_X(J,K)$ with $F_X(J,K) + \Delta F_X(J,K)$, an array of concentrations which represents the concentration profile one would expect to observe under these conditions after Δt seconds is generated.

Calculation of current.—The fractional flux of a species, Z, moving from a $J = 2$ box into a $J = 1$ box is given by

$$FF_Z(K) = DM_Z[F_Z(2,K) - F_Z(1,K)] \quad [43]$$

The contribution to the current from a given box, K, can be expressed as

$$i(K) = [FF_Z(K)](C^o_A)[A(K)\Delta X](n\mathbf{F})/\Delta t \quad [44]$$

where $A(K)$ is the area of the Kth box (thus $A(K)\Delta X$ is the volume of that box). Rearranging and substituting for ΔX and Δt we get

$$i(K)/n\mathbf{F}C^o_A = FF_Z(K)\, A(K)\, D_Z^{1/2} DM_Z^{-1/2} L^{1/2} t_k^{-1/2} \quad [45]$$

Substituting for t_k and rearranging we have

$$i(K)/(0.51)^{1/3} n\mathbf{F}C^o_A D_Z^{2/3}\omega^{1/2}\nu^{-1/6} = FF_Z(K)\, A(K)\, L^{1/2} DM_Z^{-1/2} \quad [46]$$

If we divide both sides of Eq. [46] by the area of the disk electrode, A_D, we have

$$i(K)/(0.51)^{1/3} n\mathbf{F}A_D C^o_A D_Z^{2/3}\omega^{1/2}\nu^{-1/6} = FF_Z(K) L^{1/2} DMZ^{-1/2} A(K)/A_D \quad [47]$$

Both sides of Eq. [47] are now dimensionless and the simulation variables are all on one side of the equation.

Equation [47] can be used to calculate the current at the disk electrode. That is

$$i_d/(0.51)^{1/3} n\mathbf{F}A_D C^o_A D_A^{2/3}\omega^{1/2}\nu^{-1/6} = FF_A(1)\, L^{1/2} DM_A^{-1/2} \quad [48]$$

In the case of a potential step to the limiting current plateau, since $F_A(1,1) = 0.0$, the fractional flux becomes

$$FF_A(1) = DM_A F_A(2,1) \quad [49]$$

The dimensionless parameters on each side of Eq. [48] are called ZD. Thus, in terms of experimental variables

$$ZD = i_d/(0.51)^{1/3} n\mathbf{F}A_D C^o_A D_A^{2/3}\omega^{1/2}\nu^{-1/6} \quad [50]$$

while in terms of the simulation

$$ZD = DM_A^{1/2} F_A(2,1)\, L^{1/2} \quad [51]$$

Similarly, the current at the ring electrode can be calculated. Using Eq. [47]

$$i_r/(0.51)^{1/3} n\mathbf{F}A_D C^o_A D_B^{2/3}\omega^{1/2}\nu^{-1/6} = L^{1/2} DM_B^{-1/2} \sum_{K_R} FF_B(K) A(K)/A_D \quad [52]$$

where the summation is over all radial boxes, K, corresponding to the ring electrode.

The dimensionless parameter on each side of Eq. [52] are called ZR. Thus, in terms of experimental variables

$$ZR = i_r/(0.51)^{1/3} n\mathbf{F}A_D C^o_A D_B^{2/3}\omega^{1/2}\nu^{-1/6} \quad [53]$$

while in terms of simulation variables

$$ZR = L^{1/2} DM_B^{-1/2} \sum_{K_R} FF_B(K)\, A(K)/A_D \quad [54]$$

If the potential at the ring is such that all B reaching the ring is instantly converted into A, then $F_B(1,K_R) = 0.0$ and Eq. [43] becomes

$$FF_B(K_R) = DM_B F_B(2,K_R) \quad [55]$$

Therefore, Eq. [54] becomes

$$ZR = L^{1/2} DM_B^{1/2} \sum_{K_R} F_B(2,K)\, A(K)/A_D \quad [56]$$

Note that

$$ZR/ZD = (i_r/i_d)(D_A/D_B)^{1/2} \quad [57]$$

The quotient i_r/i_d is the collection efficiency, N. Thus

$$ZR/ZD = N(D_A/D_B)^{1/2} \quad [58]$$

Though it is not necessary to do so, we will assume that $D_A = D_B$, and thus

$$ZR/ZD = N \quad [59]$$

Redefinition of boundary conditions.—At this point, the first iteration in the calculation is completed. It is now necessary to modify the boundary conditions at the disk and ring electrodes as follows.

At the disk

$$F_A'(1,1) = 0.0 \quad [60]$$

$$F_B'(1,1) = F_B(1,1) + DM_A[F_A(2,1)] - DM_B[F_B(1,1) - F_B(2,1)] \quad [61]$$

$$F_X'(1,1) = F_X(1,1) - DM_X[F_X(1,1) - F_X(2,1)] \quad [62]$$

Equation [61] states that the new fractional concentration of B at the disk, $F_B'(1,1)$, is the old fractional concentration of B at the disk, $F_B(1,1)$, plus the amount of A which diffused into the disk and is transformed (with passage of current) into B, less the B which diffuses out.

Equation [62] states that the new concentration of X at the disk, $F_X'(1,1)$, is given by the old concentration less the X which diffuses out.

The new boundary conditions at the ring electrode are

$$F_A'(1,K_R) = F_A(1,K_R) + DM_B[F_B(2,K_R)] - DM_A[F_A(1,K_R) - F_A(2,K_R)] \quad [63]$$

$$F_B'(1,K_R) = 0.0 \quad [64]$$

$$F_X'(1,K_R) = F_X(1,K_R) - DM_X[F_X(1,K_R) - F_X(2,K_R)] \quad [65]$$

At this point the calculation of the effects of diffusion, convection and kinetics are repeated, then currents are calculated at $t = 2\Delta t$, and the process is continued until steady state is reached.

Boundary conditions for constant current.—It is also of interest to simulate the application of a constant current step to the disk electrode. This is done simply by modifying the disk electrode boundary condition in the above simulation. The boundary conditions for constant current at the disk are given by

$$F_A'(1,1) = F_A(1,1) - \text{FLUX} - DM_A[F_A(1,1) - F_A(2,1)] \quad [66]$$

$$F_B'(1,1) = F_B(1,1) + \text{FLUX} - DM_B[F_B(1,1) - F_B(2,1)] \quad [67]$$

$$F_X'(1,1) = F_X(1,1) - DM_X[F_X(1,1) - F_X(2,1)] \quad [68]$$

where F_A', F_B', and F_C' are the new fractional concentrations of species A, B, and C; F_A, F_B, and F_C are the old fractional concentrations. FLUX is the amount of A transformed into B by electrolysis during each Δt interval and is given by

$$\text{FLUX} = (i_{cc}/i_L)\ (0.776)\ (DM_A/L)^{1/2} \quad [69]$$

where i_{cc} is the applied constant current and i_L is the limiting current for species A.

Results

A Fortran program based on the methods of the previous section was written; a listing and discussion of this program is available (16). Calculations for a number of different electrode geometries were carried out on a Control Data Corporation Model 6600 computer and processing times quoted refer to compilation and execution times on this.

Effect of number of iterations.—From Eq. [12] and [22] it is clear that the number of iterations, L, determines the magnitude of Δx and Δt; the larger L, the closer the simulation will approximate the physical system. A simple test of the simulation is to compare the computed steady state current at the disk with that predicted by the Levich equation (15)

$$i_{S.S.} = 0.62\, nFAC^{o}D^{2/3}\omega^{1/2}\nu^{-1/6} \quad [70]$$

When $L = 50$, the simulated steady-state current at the disk electrode is only 96.5% of the Levich equation limiting current. When $L = 1000$, however, the simulated disk current is 99.5% of the theoretical current. Similar results are obtained for the simulated collection efficiency. A simulation with $L = 50$ yields a collection efficiency 9% higher than that predicted by Albery and Bruckenstein (3) for an electrode with $IR1 = 83$, $IR2 = 94$, and $IR3 = 159$. When $L = 1000$, the simulated collection efficiency agrees to within 0.5% with the theoretical value.

Unfortunately, the computation time required to attain the steady state when $L = 1000$ is prohibitively long, requiring about 25 min of computer time. It was found, however, that identical results could be obtained from a simulation with $L = 50$, which requires only 25 sec of computer time, if a slight modification is made in the calculation of the effects of convection.

If Eq. [27] and [35] are modified as follows

$$XJJ = XJ/[1.0 - (1.11 \cdot XJ \cdot V_{NAUT})] \quad [71]$$

$$RKK = RK \exp[-1.03(XJ)(V_{NAUT})] \quad [72]$$

the results obtained with $L = 50$ are in close agreement with those using $L = 1000$ and the unmodified convection equations. The introduction of adjustable parameters into digital simulations involving convection has been successful in other cases (13). Note that the factors in Eq. [71] and [72] are valid only for $L = 50$ and $DM_A = 0.45$. There will be slightly different factors for different values of these parameters.

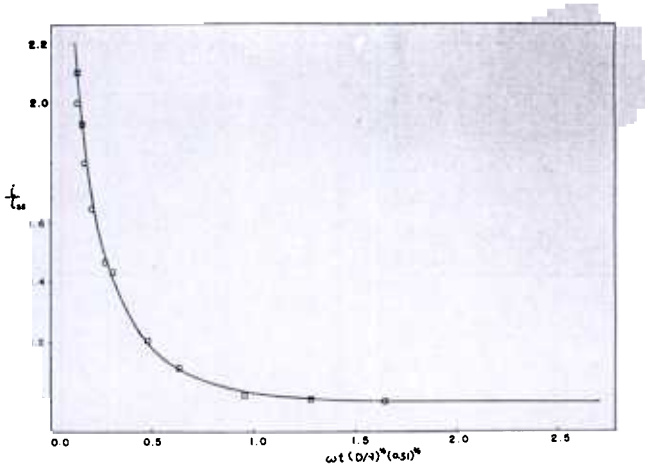

Fig. 2. Simulated disk current transient for potential step at disk: ⊙ theoretical work of Bruckenstein and Prager (17); ⊡ theoretical work of Siver (18).

Figure 2 shows the simulated disk current transient. The solid line is actually two curves, one generated using $L = 1000$ and the other using $L = 50$ and the correction factors. For all practical purposes, they are identical. The simulated curve is also compared with the theoretical and experimental work of Prager and Bruckenstein (17) and the approximate treatment of Siver (18). Both are in good agreement with the simulation.

Figure 3 shows the concentration profile of species A at steady state as a function of distance from the electrode surface in the normal direction. Curves b and c are the results of simulations using $L = 1000$, and $L = 50$ and the correction factors, respectively. On this scale, they are indistinguishable. Curve a is the theoretical concentration profile given by Riddiford (19). The agreement is quite satisfactory and indicates that the correction factors do not adversely affect the concentration profile.

Collection efficiencies.—Table I presents the simulated collection efficiencies in the absence of kinetics for a number of different electrode geometries. In these calculations $L = 50$ and the correction factors given in Eq. [71] and [72] were used. In all cases the simulated collection efficiencies are in excellent agreement with the theoretical collection efficiencies of Albery and Bruckenstein (3). Identical steady-state collection efficiencies are also predicted when the boundary conditions at the disk electrode correspond to a constant current step rather than a potential step. This is as would be expected. Furthermore, the steady-state collection efficiencies are unaffected by the mag-

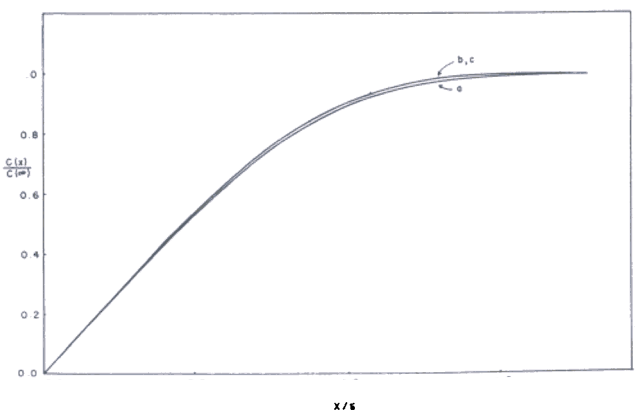

Fig. 3. Concentration profile of species at the disk: a, theoretical curve by Riddiford (19); b, simulated curve, $L = 1000$; c, simulated curve, $L = 50$, correction factors used. $\delta = 1.805\, D^{1/3}\nu^{1/6}\omega^{-1/2}$.

Table I. Simulated collection efficiencies for different electrode geometries

r_2/r_1	r_3/r_1	Collection efficiencies: Simulated[a]	Collection efficiencies: Calculated[b]
1.05	1.261	0.339	0.340
1.05	1.361	0.408	0.409
1.05	1.472	0.463	0.464
1.07	1.161	0.209	0.210
1.07	1.271	0.321	0.323
1.07	1.371	0.391	0.391
1.07	1.483	0.449	0.449
1.09	1.201	0.226	0.226
1.09	1.301	0.320	0.321
1.09	1.521	0.449	0.447

[a] $L = 50$, correction factors used. Computation time about 20 sec per calculation.
[b] Calculated from tables in (3).

nitude of the current step, provided the current is smaller than the limiting current.

Ring transients.—From an approximate treatment of ring current transients (RCT), Albery (9) suggested that these could be employed to study fast homogeneous reactions of species generated at the disk electrode. Bruckenstein and Feldman (20) introduced the concept of the transit time from disk to ring electrode and suggested its application to the determination of rate constants of homogeneous reactions. Bruckenstein and Napp (21) have also shown that the RCT can be used to determine the amount of adsorption of electrogenerated products.

Figure 4 shows the RCT obtained when either a potential step or a current step is applied to the disk electrode and the ring electrode is held at a potential where all product reaching it is electrolyzed. The computed results for the RCT are identical for $L = 1000$ or for $L = 50$ and the modified convection equations.

Note that the current at the ring rises more rapidly when a potential step is applied. This is caused by the large instantaneous current which results at the disk when the potential is stepped (Fig. 2). The RCT, normalized by the steady-state ring current, due to a current step is independent at the magnitude of the current step.

We can compare the simulated RCT's with transit times predicted by Bruckenstein and Feldman (20). The appropriate equation given by them for the transit time (the time interval between the potential step at the disk and the appearance of current at the ring) in the absence of complications is

$$\omega t' D^{1/3} \nu^{-1/3} (0.51)^{2/3} = B[\log (r_2/r_1)]^{2/3} \qquad [73]$$

where ω is in radians/sec, t' is the transit time, and r_1 and r_2 are the radii of the disk and inner edge of the ring, respectively. Bruckenstein and Feldman (20) take B = 2.87, while a slightly different method of carrying out the integration in the derivation yields B = 2.28. Figure 5 shows the simulated RCT's for a potential step at the disk for electrodes of different geometries. Also shown are the transit times calculated from Eq. [73] for B-values of 2.28 and 2.87. A useful definition of the transit time, corresponding to Eq. [73] with B = 2.28, is that time at which the current is approximately 2% of the steady-state ring current. Taking the transit time at a given fraction of the steady-state current seems preferable for many electrodes to methods involving extrapolations of the rising current region of the RCT.

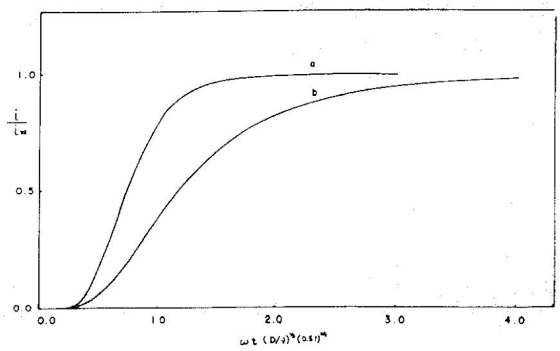

Fig. 4. Simulated ring current transients: a, potential step at the disk; b, current step at the disk; $L = 50$, correction factors used.

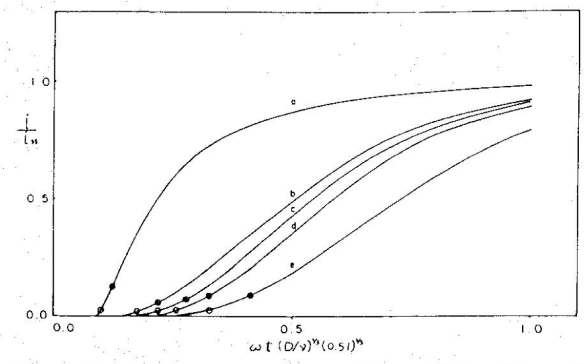

Fig. 5. Simulated transit times: a, $IR1 = 2000$, $IR2 = 2040$, $IR3 = 2080$; b, $IR1 = 100$, $IR2 = 105$, $IR3 = 147$; c, $IR1 = 100$, $IR2 = 107$, $IR3 = 148$; d, $IR1 = 100$, $IR2 = 109$, $IR3 = 152$; e, $IR1 = 83$, $IR2 = 94$, $IR3 = 159$; $L = 50$, correction factors used. The points correspond to transit times calculated using Eq. [73] with B = 2.28 (open points) and 2.87 (solid points).

We can also compare our results with those of Albery (9) who treated the RCT for the current step condition. For a thin-ring thin-gap electrode, he obtained two approximate equations, one which is valid at long times and the other which is more valid at short times. Figure 6 shows the simulated RCT for the current step condition at a fairly thin-ring thin-gap electrode ($IR1 = 2000$, $IR2 = 2040$, $IR3 = 2080$). Also plotted are points obtained from Albery's equations. The agreement is acceptable and points out the limits within which the approximate equations are valid. Unfortunately, these equations cannot be employed for most practical electrodes which are not of the required thin-ring thin-gap configuration.

Conclusion

The digital simulation technique has been shown to give theoretical results for transient and steady state behavior which are in good agreement with previous theoretical treatments and experiments. The digital simulation approach has the advantage of being directly applicable to situations involving more complex boundary conditions and coupled first and second order homogeneous chemical reactions. Results of dig-

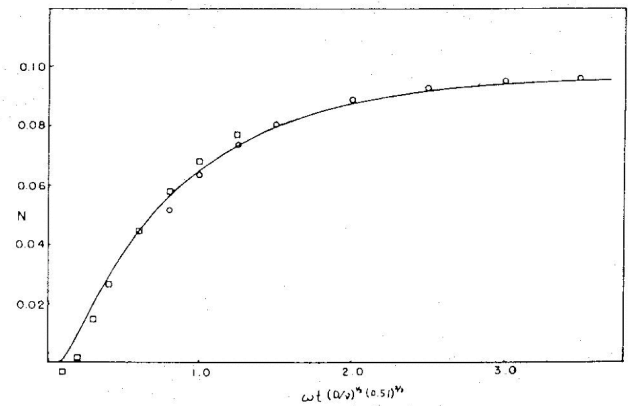

Fig. 6. Simulated current transient for thin ring-thin gap electrode with current step at the disk: $IR1 = 2000$, $IR2 = 2040$, $IR3 = 2080$; $L = 50$, correction factors used from Albery's Eq. [3.4] (9) using pre-exponential factors. ○ 0.94; □ 0.81.

ital simulations under these conditions and for electrogenerated chemiluminescence at the RRDE, and applications of these treatments, will be given in future papers.

Acknowledgment

The support of The Electrochemical Society, Mobil Oil Corporation and the Eastman Kodak Company for fellowships to one of us (K.B.P.) and the Robert A. Welch Foundation and the National Science Foundation (AP-6688X) are gratefully acknowledged. The authors are indebted to J. T. Maloy for helpful discussions during the course of this work.

Manuscript received April 18, 1969.

Any discussion of this paper will appear in a Discussion Section to be published in the December 1970 JOURNAL.

REFERENCES

1. A. N. Frumkin and L. N. Nekrasov, *Doklady Akad. Nauk. SSSR*, **126**, 115 (1959).
2. W. J. Albery, *Trans. Faraday Soc.*, **62**, 1915 (1966).
3. W. J. Albery and S. Bruckenstein, *ibid.*, **62**, p. 1920.
4. W. J. Albery, S. Bruckenstein, and D. T. Napp, *ibid.*, p. 1932.
5. W. J. Albery, S. Bruckenstein, and D. C. Johnson, *ibid.*, p. 1938.
6. W. J. Albery and S. Bruckenstein, *ibid.*, p. 1946.
7. W. J. Albery and S. Bruckenstein, *ibid.*, p. 2584.
8. W. J. Albery and S. Bruckenstein, *ibid.*, p. 2596.
9. W. J. Albery, *ibid.*, **63**, 1771 (1967).
10. W. J. Albery, M. L. Hitchman, and J. Ulstrup, *ibid.*, **64**, 2831 (1968).
11. J. T. Maloy, K. B. Prater, and A. J. Bard, *J. Phys. Chem.*, **72**, 4348 (1968).
12. S. W. Feldberg and C. Auerbach, *Anal. Chem.*, **36**, 505 (1964).
13. S. W. Feldberg, "Electroanalytical Chemistry," Vol. 3, A. J. Bard, Editor, Marcel Dekker, Inc., New York (1969).
14. W. J. Albery and J. Ulstrup, *Electrochim. Acta*, **13**, 281 (1968).
15. V. G. Levich, "Physiochemical Hydrodynamics," Prentice-Hall, Englewood Cliffs, N.J. (1962).
16. K. B. Prater, Ph.D. Dissertation, University of Texas at Austin, 1969.
17. S. Bruckenstein and S. Prager, *Anal. Chem.*, **39**, 1161 (1967).
18. Yu G. Siver, *Russ. J. Phys. Chem.*, **33**, 533 (1959).
19. A. C. Riddiford, "Advances in Electrochemistry and Electrochemical Engineering," P. Delahay and C. W. Tobias, Editors, Interscience, New York (1966).
20. S. Bruckenstein and G. Feldman, *J. Electroanal. Chem.*, **9**, 395 (1965).
21. S. Bruckenstein and D. T. Napp, *J. Am. Chem. Soc.*, **90**, 6303 (1968).